ANTIOXIDANTS & REDOX SIGNALING
Volume 28, Number 1, 2018

DOI: 10.1089/ars.2017.6992

Discoveries

ORIGINAL RESEARCH COMMUNICATION

Mitochondrial Complex I Reversible S-Nitrosation Improves Bioenergetics and Is Protective in Parkinson's Disease

Chiara Milanese,[1,2] Victor Tapias,[3,4] Sylvia Gabriels,[1] Silvia Cerri,[5] Giovanna Levandis,[5] Fabio Blandini,[5] Maria Tresini,[1] Sruti Shiva,[6,7] John Timothy Greenamyre,[3,4] Mark T. Gladwin,[8,9] and Pier G. Mastroberardino[1]

Abstract

Aims: This study was designed to explore the neuroprotective potential of inorganic nitrite as a new therapeutic avenue in Parkinson's disease (PD).
Results: Administration of inorganic nitrite ameliorates neuropathology in phylogenetically distinct animal models of PD. Beneficial effects are not confined to prophylactic treatment and also occur if nitrite is administered when the pathogenic cascade is already active. Mechanistically, the effect is mediated by both complex I S-nitrosation, which under nitrite administration is favored over formation of other forms of oxidation, and down-stream activation of the antioxidant Nrf2 pathway. Nitrite also rescues respiratory reserve capacity and increases proton leakage in LRRK2 PD patients' dermal fibroblasts.
Innovation: The study proposes an unprecedented approach based on the administration of the nitrosonium donor nitrite to contrast complex I and redox anomalies in PD. Dysfunctional mitochondrial complex I propagates oxidative stress in PD, and treatments mitigating this defect may, therefore, limit disease progression. Therapeutic complex I targeting has been successfully achieved in ischemia/reperfusion by using nitrosonium donors such as nitrite to reversibly modify its subunits and protect from oxidative damage after reperfusion. This evidence led to the innovative hypothesis that nitrite could exert protective effects also in pathological conditions where complex I dysfunction occurs in normoxia, such as in PD.
Conclusions: Overall, these results demonstrate that administration of inorganic nitrite improves mitochondrial function in PD, and it, therefore, represents an amenable intervention to hamper disease progression. *Antioxid. Redox Signal.* 28, 44–61.

Keywords: mitochondrial complex I, neurodegenerative disorders, neuroprotection, nitrite, Parkinson's disease

Introduction

Parkinson's disease (PD) is the prototypical movement disorder and is characterized by a progressive deterioration of the dopaminergic (DA) nigrostriatal circuits. A small fraction of PD cases are familial and attributable to single monogenic mutations; the vast majority of the disease, however, is sporadic and its etiology includes complex interactions between genetic and environmental factors. PD is a disease of advancing age, and clinical manifestations appear relatively late in life; tremors, bradykinesia, postural instability, and rigidity are PD pathognomonic signs and manifest when a large

[1]Department of Molecular Genetics, Erasmus MC, Rotterdam, The Netherlands.
[2]Ri.MED Foundation, Palermo, Italy.
[3]Department of Neurology, University of Pittsburgh, Pittsburgh, Pennsylvania.
[4]Pittsburgh Institute for Neurodegenerative Diseases, University of Pittsburgh, Pittsburgh, Pennsylvania.
[5]Laboratory of Functional Neurochemistry, Center for Research in Neurodegenerative Diseases, C. Mondino National Neurological Institute, Pavia, Italy.
[6]Vascular Medicine Institute, University of Pittsburgh, Pittsburgh, Pennsylvania.
[7]Department of Pharmacology and Chemical Biology, University of Pittsburgh, Pittsburgh, Pennsylvania.
[8]Pittsburgh Heart, Lung, Blood and Vascular Medicine Institute, University of Pittsburgh, Pittsburgh, Pennsylvania.
[9]Division of Pulmonary, Allergy and Critical Care Medicine, Department of Medicine, University of Pittsburgh, Pittsburgh, Pennsylvania.

Innovation

Parkinson's disease (PD) is a neurodegenerative disorder significantly affecting quality of life. Strategies to cure it, or even to slow down its progression, are not available and therapies are limited to symptoms' palliation.

We demonstrate that administration of inorganic nitrite mitigates neuropathology in multiple PD models. Mechanistically, nitrite improves mitochondrial function and activates endogenous antioxidant defenses. Nitrite also corrects impaired mitochondrial bioenergetics in patients' fibroblasts.

Our study indicates that nitrite holds clinical potential as a novel therapeutic agent for PD. Nitrite is currently tested in clinical studies to treat cardiovascular conditions, and it could, therefore, be easily repositioned for PD treatment.

proportion ($\sim 50\%$) of DA neurons are lost (41). At present, no effective cure for PD is available and therapies are limited to palliation of symptoms. Conventional wisdom has it that treatments retarding neuronal loss and preventing development of large lesions would be of great benefit for patients because they would arrest symptomatic deterioration. In view of the complexity of PD pathogenesis, which perturbs multiple cellular pathways, simultaneous targeting of different processes would increase the chance of therapeutic success.

Defects in mitochondrial respiratory complex I and oxidative stress have been consistently associated with PD by laboratory, clinical, and epidemiological studies, and they are mechanistically interconnected (8, 68, 69). Complex I inhibition, in fact, results in increased production of mitochondrial reactive oxygen species (ROS) (66), which, in turn, may attack complex I amino acid residues in a positive feedback loop to generate irreversible damage (56) that exacerbates deterioration. Complex I, therefore, represents a tractable target in PD.

Targeting of complex I for therapeutic purposes has been principally explored in hypoxic pathological conditions, such as cardiac ischemia/reperfusion injury (20, 67). These approaches relied on nitric oxide (NO)-mediated modification of complex I, which favors reversible over irreversible thiol oxidation and prevents its abrupt reactivation during reperfusion, limiting the burst in ROS intrinsically associated with re-oxygenation (20, 67). This strategy is, therefore, based on induction of preventive mild oxidation, emulates traditional preconditioning, and leads to significant mitigation of infarct size.

Inorganic nitrite is a biological reservoir for NO, which is produced after nitrite reduction by myoglobin, hemoglobin, neuroglobin, and/or xanthine oxidoreductase (45, 46). Nitrite has been shown to restore NO signaling and confer protection in ischemia/reperfusion *via* complex I reversible S-nitrosation in multiple independent studies and in several organs, including liver, heart, and brain (45, 60). NO depletion and derangement of NO-mediated signaling also occurs during aging and under oxidative stress (45). Investigations of nitrite-induced protective effects have shown that—even in normoxic conditions—nitrite increases tolerance to subsequent ischemia/reperfusion with a mechanism that modulates mitochondrial physiology and activates protein kinases (39). These findings suggest that nitrite deserves consideration also in the treatment of other conditions, particularly those where complex I defects and oxidative stress play prominent pathogenic roles. PD largely fulfills these criteria.

This study interrogated the potential of nitrite in normoxic conditions, as a neuroprotective agent in PD, in multiple and phylogenetically diverse animal models, from zebrafish to rodents. We examined the underlying mechanisms in a cellular model of DA degeneration and translated our findings to human cases by studying nitrite effects on primary dermal fibroblasts from familial PD patients with *LRRK2* mutations, which are the most common variants associated with this disease (42). Collectively, our data show that nitrite slows PD progression and, therefore, holds clinical potential as a disease-modifying agent.

Results

Nitrite administration is protective in multiple preclinical animal models of PD

In a preliminary investigation, the potential of nitrite administration in PD was assessed in the small vertebrate zebrafish, which is a well-described model of PD (11, 12, 30, 50, 57). Two days treatment of larvae with the DA toxin MPP^+—the active metabolite of the prototypical PD toxin 1-Methyl-4-phenyl-1,2,3,6-tetrahydropyridine hydrochloride (MPTP)—results in selective degeneration of ascending DA neurons in the posterior tuberculum (PT), the homologue structure of the *substantia nigra* pars compacta (SNpc) in zebrafish (40, 63, 65) (Fig. 1B, C, F–G). Administration of

FIG. 1. Nitrite ameliorates MPP^+ effects on TH-immunoreactive neurons in zebrafish larvae. **(A)** Schematic of the experimental design: 1 dpf embryos were treated with nitrite dissolved in E3 water for 4 days. The compound was then removed, and the larvae were exposed for 48 h to 1 m*M* MPP^+. **(B)** Sagittal overview of the zebrafish brain showing the localization of the PT. CCe, corpus cerebelli; Hyp, hypothalamus; Mo, medulla oblongata; MS, medulla spinalis; Ob, olfactory bulb; Tel, telencephalon; TeO, tectum opticum. **(C)** Exposure to MPP^+ reduces the number of TH-positive neurons in the posterium tuberculum (PT); 4 days nitrite pretreatment (1 and 10 μM) significantly prevents neuronal cell loss. **(D–K)** Representative images of a sagittal overview of TH-positive neuronal clusters distribution in 7 dpf zebrafish larvae brains exposed to nitrite **(H–K)** and MPP^+ **(F–K)** treatments. The catecholaminergic clusters in the PT are magnified in the *insets* **(E, G, I, K)**. Scale bars: 50 μm. **(L–N)** Spontaneous motor activity of 7 dpf zebrafish larvae exposed to nitrite and/or MPP^+. **(L)** Representative image of the characteristic swimming pattern of larvae in a single-larva/single-well setup after treatments. Activity is expressed in terms of mean velocity **(M)** and percentage of time spent moving **(N)** in a 2 h-recording time frame. Results shown in **(C)** are based on two independent technical replicates, and results shown in **(M, N)** represent four independent technical replicates ($*p<0.05$; $**p<0.01$; $***p<0.001$; one-way ANOVA followed by Dunnett's multiple-comparison *post hoc* test). Graphs represent mean ± SEM. ANOVA, analysis of variance; dpf, days postfertilization; SEM, standard error of the mean; TH, tyrosine hydroxylase.

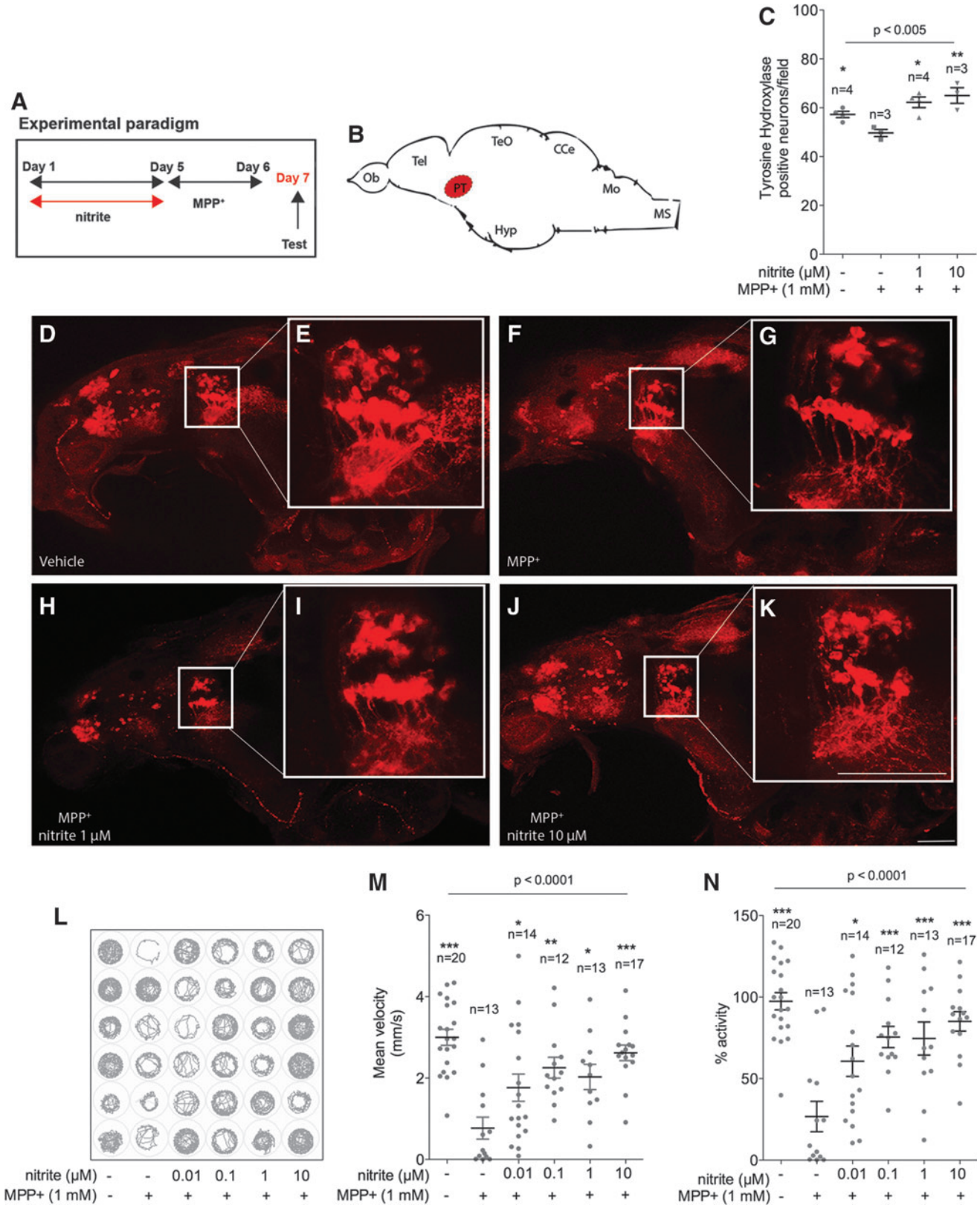

MPP^+ constitutes an appropriate experimental setting for preliminary investigation of the neuroprotective potential of nitrite because it inhibits mitochondrial complex I (61) and causes redox imbalance (59). Due to its distinctive sensitivity to MPP^+, the Tupfel long fin (TL) zebrafish strain was selected for the study (13). To exclude direct pharmacological interaction between nitrite and MPP^+, the former was removed from the medium before addition of the neurotoxin (Fig. 1A). DA toxicity was evaluated by counting neurons in the ventral diencephalic clusters and the associated behavioral anomalies by measuring spontaneous motor activity and swimming velocity. As expected, 1 m*M* MPP^+ treatment for two consecutive days, starting at 5 days postfertilization (dpf), induced significant loss of DA neurons in the PT (Fig. 1C) paralleled by a sharp decrease in locomotor activity (Fig. 1L–N). Four days pretreatment with nitrite dissolved in E3 medium, starting at 1 dpf, resulted in dose-dependent neuroprotection and improvement in locomotor activity (Fig. 1C, L–N).

We next sought evidence for nitrite neuroprotection rodents. As expected, nitrite administration induces transient S-nitrosation of proteins extracted from the ventral mesencephalic region containing the SNpc (Supplementary Fig. S1; Supplementary Data are available online at www.liebertpub.com/ars). Initially, we focused on the chronic progressive rotenone rat PD model. Chronic administration of low doses of rotenone results in systemic inhibition of complex I, which, in turn, recapitulates essential features of PD, including selective degeneration of SNpc DA neurons, oxidative stress, alpha-synuclein pathology, and gastrointestinal neuropathology (8, 18, 26, 37, 48). Indeed, nitrite administration in drinking water—initiated 72 h before the first rotenone injection and continued until the end of the treatment (Fig. 2A)—preserved DA projections in the striatum (Fig. 2B, D) and significantly reduced loss of DA neurons in the SNpc, as demonstrated by unbiased stereological counts (Fig. 2C, E).

To further substantiate the neuroprotective potential of nitrite in PD, investigations were extended to the 6-hydroxydopamine (6-OHDA) rat model, in which pathology is experimentally induced by a unilateral intrastriatal injection of this toxin. This leads to progressive nigrostriatal degeneration (9), caused by oxidative stress and by inhibition of complex I dependent mitochondrial respiration (34, 35). Importantly, the 6-OHDA model has been used to screen potential neuroprotectants and all the drugs currently used in clinical practice effectively ameliorate motor symptoms in 6-OHDA-treated rats, with the only exception of antimuscarinic compounds (27). Initial experiments addressed the effects of acute administration of nitrite (2 mg/kg), which was injected in rats 24 and 1 h before stereotaxic infusion of 6-OHDA (Fig. 2F, top panel). Treatment resulted in significant reduction of the DA lesion (Fig. 2G–I, acute). Subsequent experiments evaluated the effects of chronic treatment, where nitrite was administered for 3 weeks in drinking water (50 mg/L), starting 7 days after 6-OHDA infusion (Fig. 2F, lower panel), when degeneration of the nigrostriatal pathways is already pronounced (10). Nitrite administration also successfully mitigated DA degeneration in this experimental setup (Fig. 2G–I, chronic).

Nitrite effects in human PD

We next explored whether the nitrite effects observed in PD preclinical models could be translated to human pathobiology. We investigated mitochondrial function in dermal fibroblasts obtained from biopsies of patients harboring LRRK2 mutations (Table 1) (3, 7, 23, 47), and we used a Seahorse Extracellular Flux Analyzer to characterize the bioenergetics profile of these cells (Fig. 3A). Out of the three studied PD lines, only one (ND32976) exhibited reduced basal respiration (Fig. 3B). However, rotenone-sensitive respiration reflecting complex I activity was decreased in all PD samples (Fig. 3C), substantiating the central role of mitochondrial complex I defects also in genetic PD (23). Respiratory reserve capacity, which modulates the response to stress-induced pathology (36), was also decreased in all specimens (Fig. 3D). Pretreatment with nitrite (48 h) led to significant improvement in both rotenone-sensitive respiration and reserve capacity (Fig. 3F, G) in two of the LRRK2 mutant lines, but it had no effect on cell lines from controls (Table 1). In addition, nitrite pretreatment significantly decreased basal H^+ leakage in *LRRK2* samples (Fig. 3E)—therefore improving mitochondrial efficiency—in agreement with previous observations (43); interestingly, nitrite augmented H^+ leakage in control cells.

Effects of nitrite on MPP^+-treated SH-SY5Y cells

To determine the mechanisms of action of nitrite-mediated neuroprotection observed *in vivo*, we performed experiments in the SH-SY5Y DA cell line, which is commonly used as an *in vitro* model of PD (66).

Mechanisms affecting cell survival and protein redox state

Consistent with previous data (4, 28, 66), administration of MPP^+ affected cell survival, which was significantly ameliorated by nitrite (Fig. 4A–C). Treatment with nitrite alone did not induce cell death and protection was completely abolished by the NO scavenger carboxy-PTIO, thus confirming that the observed effect was mediated by nitrite-derived NO (Fig. 4B, C).

Nitrite induced an increase in protein S-nitrosation in MPP^+ treated SH-SY5Y, consistent with augmented nitrite-dependent S-nitrosation (Fig. 4D, E, compare lanes 2, 3, and 5 and Supplementary Fig. S2), whereas MPP^+ alone did not alter S-nitrothiol levels (Fig. 4D, E, compare lanes 1 and 2). In nitrite/MPP^+ co-treated samples, administration of the NO scavenger carboxy-PTIO abolished the observed increase in S-nitrosothiol formation (Fig. 4D, E, compare lanes 3, 4, 5, and 6). Replacement of nitrite with the NO donor 3,3-Bis(aminoethyl)-1-hydroxy-2-oxo-1-triazene (NOC-18), which ensures sustained NO release because of its long half-life (21), led to comparable results and further confirmed the central role of NO in the observed effects (Fig. 4D, E, compare lanes 7 and 8).

Next, we explored whether increased reversible S-nitrosation could protect cysteine thiols from higher oxidation states (*i.e.,* sulfinic and sulfonic acids), which can cause functional anomalies in proteins and also predispose them to aggregation (62). Protein sulfenic acid formation induced by hydrogen peroxide (H_2O_2) was significantly lessened by nitrite pretreatment (Fig. 4F, G), confirming that nitrite treatment favors reversible over irreversible thiol modification in proteins.

Nitrite administration did not abolish production of mitochondrial superoxide (Fig. 4H), in agreement with previous studies showing that mitochondrial ROS production is

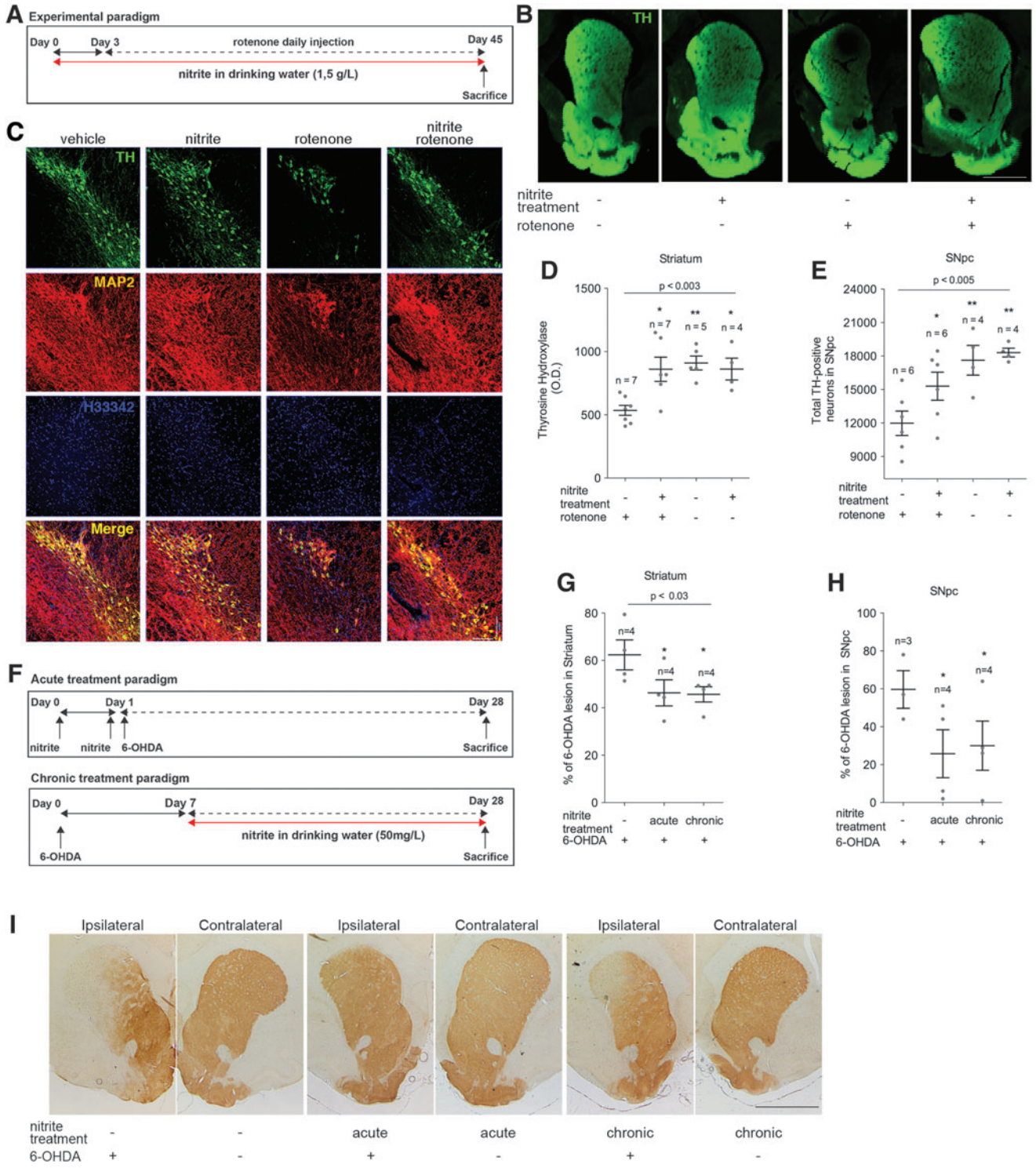

FIG. 2. Nitrite administration ameliorates pathology in rotenone and 6-OHDA rat models of PD. **(A)** Schematic of the experimental paradigm for nitrite and rotenone administration. **(B)** Representative image of striatal TH immunohistochemistry reveals severe depletion in DA fibers after rotenone exposure, which is strongly mitigated on treatment with inorganic nitrite (scale bar: 1 mm). **(C)** Representative image of rotenone-induced DA loss in the SNpc, which is prevented by nitrite co-treatment (scale bar: 100 μm). **(D)** Quantification of striatal innervation in **(B)** by densitometry. **(E)** Quantification of DA loss in the SNpc **(C)** by unbiased stereological counts. **(F)** Experimental 6-OHDA setup: In the *acute paradigm* (*top*), nitrite was administered 24 and 1 h before stereotactic infusion in the rat striatum; in the *chronic paradigm* (*bottom*), nitrite was administered orally, dissolved in drinking water, starting 7 days after induction of the lesion. **(G, H)** Nitrite administration ameliorates the 6-OHDA-induced lesions in striata and in SNpc. **(I)** Representative images of striata cross-sections injected with 6-OHDA (*ipsilateral*) and the respective untreated side (*contralateral*) of nitrite-treated rats (Scale bar: 1 mm) ($*p < 0.05$; $**p < 0.01$; one-way ANOVA followed by Dunnett's multiple-comparison *post doc* test for **D, E, G**; two-sided Student's *t*-test for **H**). Graph represents mean ± SEM. 6-OHDA, 6-hydroxydopamine; DA, dopaminergic; PD, Parkinson's disease; SNpc, *substantia nigra* pars compacta.

Table 1. Parkinson's Disease Patients' and Controls' Related Information

Description	*Gender*	*Age*	*Race*	*Affected*	*Gene*	*Mutation*
ND32975	Female	74	Caucasian	Yes	*LRRK2*	ARG1441GLY
ND32976	Female	69	Caucasian	Yes	*LRRK2*	ARG1441GLY
ND33879	Female	66	Caucasian	Yes	*LRRK2*	GLY2019SER
AG08269	Female	82	Caucasian	No	No	No
CHDF	Male	62	Caucasian	No	No	No

required for nitrite-mediated cytoprotection under normoxic conditions (39).

Mitochondrial respiration and complex I thiol redox status in MPP$^+$-treated SH-SY5Y

The SH-SY5Y cell line was also used to evaluate the effects of nitrite administration on the recovery of mitochondrial respiration after transient MPP$^+$ challenge (25). Four-hour exposure to MPP$^+$ significantly suppressed basal mitochondrial respiration, and toxin removal was not sufficient to promote full recovery. Contrastingly, samples pretreated with nitrite successfully restored respiration to control levels (Fig. 5A).

Next, the redox equilibrium between S-nitrosated and reduced cysteines was examined in immunocaptured complex I.

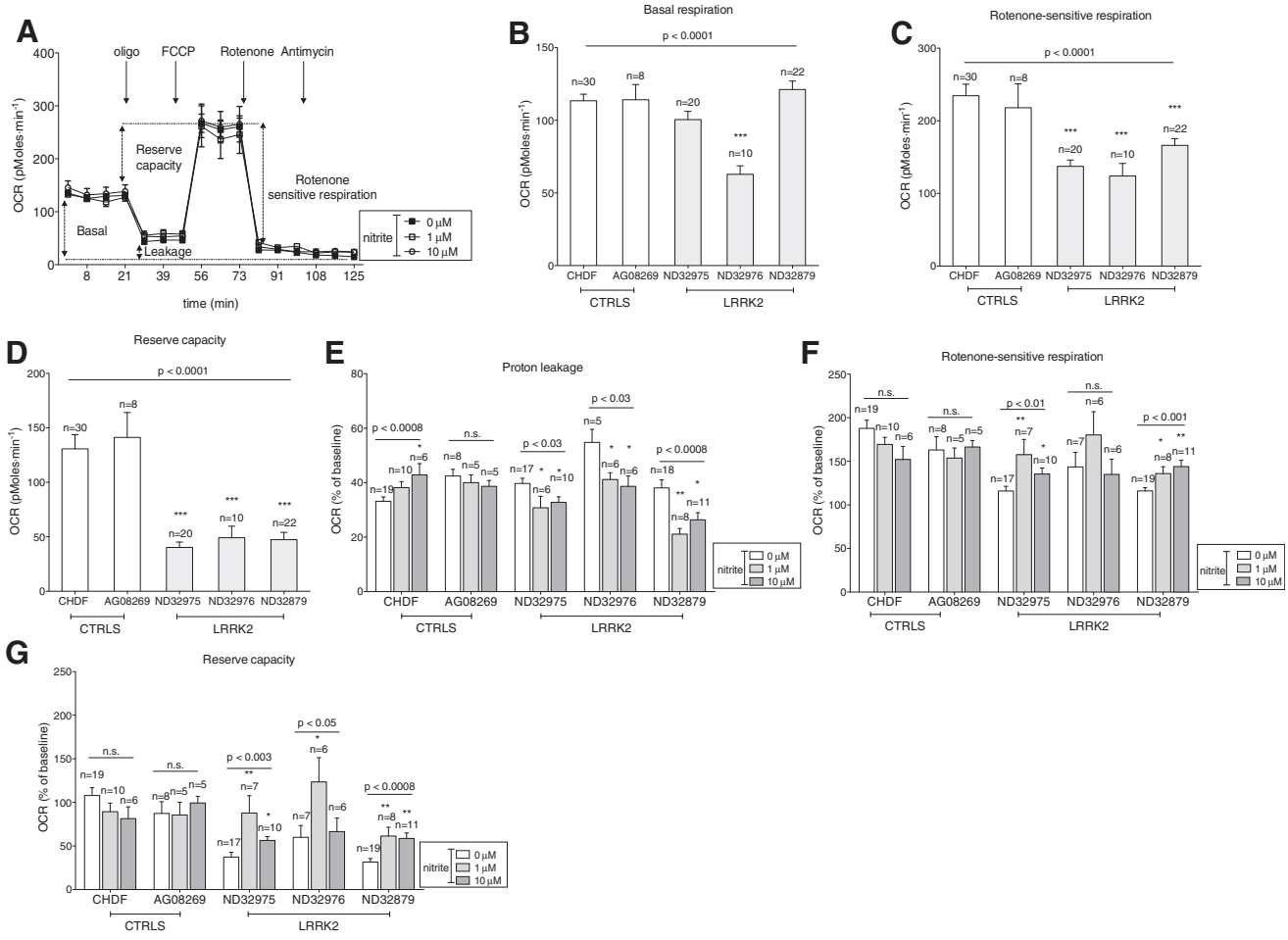

FIG. 3. Nitrite improves mitochondrial respiration in dermal fibroblasts from PD patients harboring LRRK2 mutations. **(A)** Oxygen consumption rate (OCR) profile of fibroblast from healthy subjects pretreated 48 h with nitrite (1 or 10 μM). Fibroblasts were challenged with sequential administration of oligomycin to inhibit ATP synthase, FCCP to elicit maximal respiration, rotenone to inhibit complex I, and antimycin to inhibit complex III and fully block respiration. The parameters analyzed in the profile were: basal respiration, proton leakage, mitochondrial reserve capacity (as difference between maximum reserve capacity and basal respiration), and rotenone sensitive respiration, which accounts for the respiration dependent on complex I. **(B–D)** Quantification of basal OCR levels **(B)**, rotenone sensitive respiration **(C)**, and reserve capacity **(D)** of fibroblasts derived from healthy controls and *LRRK2*-PD patients. **(E–G)** Administration of nitrite significantly improves mitochondrial respiration in PD fibroblast by decreasing proton leakage **(E)**, increasing the rotenone-sensitive respiration **(F)** and reserve capacity **(G)**. OCR values are expresses as% of variation from the baseline. Results are based on three independent experiments ($*p<0.05$; $**p<0.01$; $***p<0.001$; one-way ANOVA followed by Dunnett's multiple-comparison *post doc* test). Graphs represent mean ± SEM.

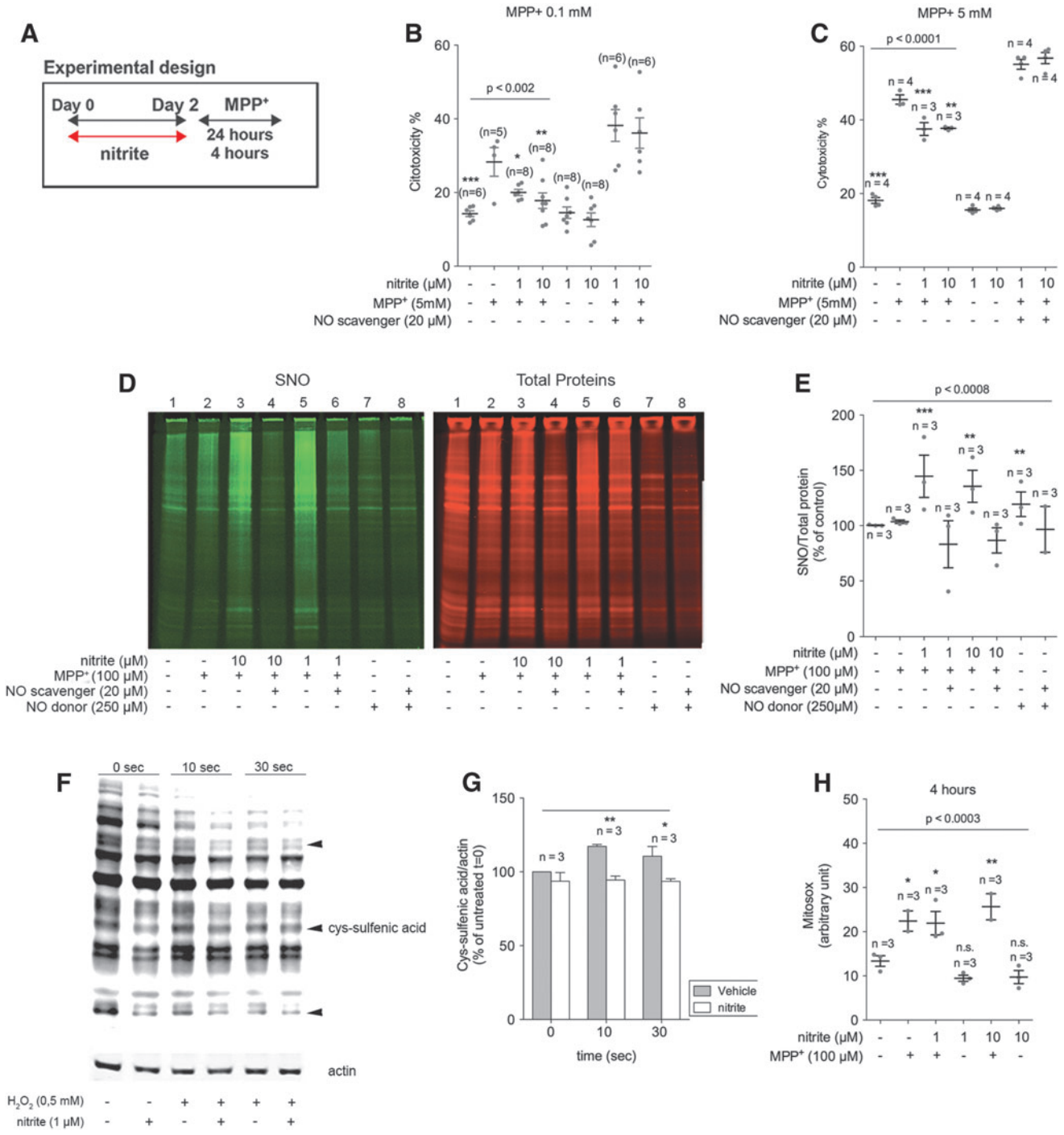

FIG. 4. Mechanisms underlying nitrite cytoprotection. **(A)** Experimental design; after 48 h of incubation, nitrite was removed from the medium and SH-SY5Y cells were exposed to MPP^+. **(B, C)** Effects of nitrite pretreatment on MPP^+ cytotoxicity (100 μM in **B** and 5 mM in **C**); nitrite administration significantly reduces cell death. **(D)** Representative image of the in-gel detection of protein S-nitrosation (SNO) after MPP^+ (100 μM) and/or nitrite treatment. Free cysteine thiols were blocked with NEM, and S-nitrosated cysteines were labeled with fluorescent NEM after reduction with ascorbate and Cu^{++} (SNO, *green* signal). As a loading control, total proteins were labeled with NHS-ester (*red* signal). **(E)** Although MPP^+ exposure does not induce changes in protein S-nitrosation, pretreatment with nitrite significantly increases SNO levels. **(F, G)** H_2O_2 induces rapid formation of sulfenic acid on cysteines, which is prevented by nitrite-mediated S-nitrosation pretreatment. SH-SY5Y cells were treated with 0.5 mM H_2O_2 and lysed in the presence of dimedone. Nitrite pretreaded samples showed reduced formation of dimedone adducts (*arrowheads* in **F**—representative image). The bar graph **(G)** represents densitometric analysis of the whole lane normalized over actin. **(H)** Superoxide production in SH-SY5Y exposed to 4 h of 100 μM MPP^+. Nitrite pretreatment does not prevent the increase in superoxide production induced by MPP^+ exposure. Results are based on three independent experiments ($*p<0.05$; $**p<0.01$; $***p<0.001$; one-way ANOVA followed by Dunnett's multiple-comparison *post doc* test). Graphs represent mean ± SEM. H_2O_2, hydrogen peroxide; NEM, N-Ethylmaleimide; NHS, normal horse serum.

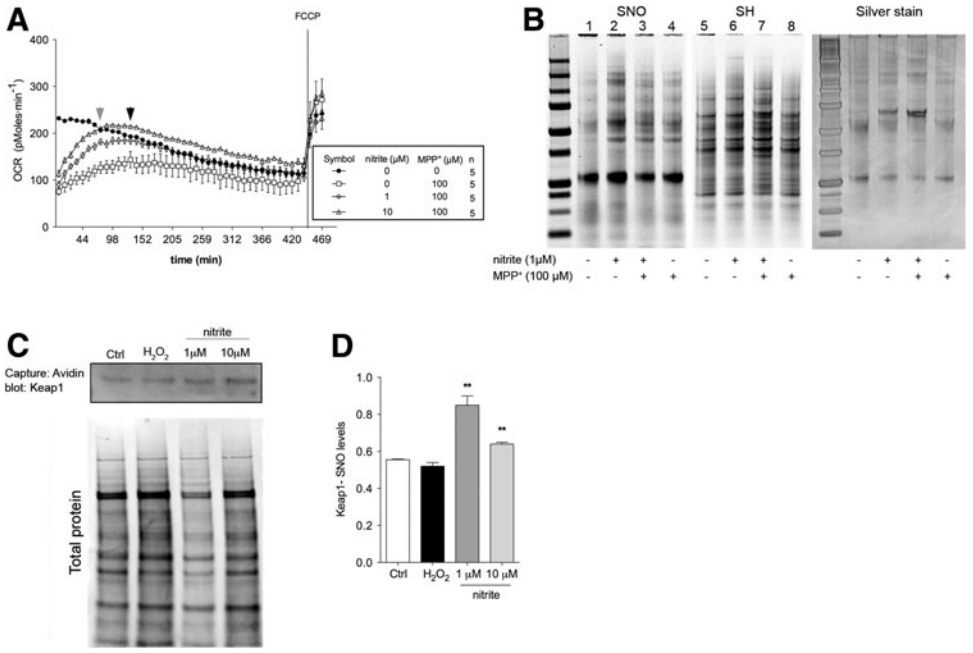

FIG. 5. Nitrite pretreatment improves the recovery of mitochondrial respiration and induces Keap1 S-nitrosation. **(A)** Nitrite administration stimulates recovery of mitochondrial respiration after a transient 4 h exposure to MPP^+. SH-SY5Y cells were seeded in a Seahorse Bioscience V7 tissue culture plate, incubated with nitrite for 48 h, and finally treated with 100 μM MPP^+. After 4 h, MPP^+ was removed and basal OCR was monitored for 8 h with a Seahorse XF24 Extracellular Flow Analyzer. Nitrite pretreated cells reached control OCR levels after 76 (10 μM, *gray arrowhead*) and 130 (1 μM, *black arrowhead*) minutes, whereas respiration in cells treated only with MPP^+ remained consistently lower than controls. **(B)** Representative in-gel detection of S-nitrosated (SNO, *left panel*) and reduced (SH, *central panel*) cysteine thiols in immunocaptured mitochondrial complex I extracted from cells treated with nitrite and/or MPP^+ reveals reduction of mitochondrial complex I protein cysteines in MPP^+ specimen pretreated with nitrite (compare lane 7 with other lanes). Gel protein loading was assessed by silver staining (*right panel*). **(C, D)** Nitrate administration induces S-nitrosation of Keap1. SH-SY5Y cells received a 48 h treatment with nitrite (1 or 10 μM) or a 30′ treatment with H_2O_2 (0.5 mM), and the biotin switch reaction was performed in all samples in the presence of biotin-NEM, Cu^{++}, and ascorbate. Biotinylated proteins were captured with streptavidin-conjugated beads, separated on a gel, and probed with an anti-Keap1 antibody (C, representative image, full gel in Supplementary Fig. S3). S-nitrosated-Keap1 levels were normalized on the precaptured SNO-modified total lysates labeled with NHS-ester **(D)**. $^{**}p < 0.01$; one-way ANOVA followed by Dunnett's multiple-comparison *post doc* test. Graphs represent mean ± SEM.

Nitrite increased S-nitrosation without altering levels of reduced cysteines (Fig. 5B, compare lanes 2 and 6). However, when nitrite was co-administered with MPP^+, S-nitrosation was paralleled by a marked increment in reduced cysteine-thiol levels (Fig. 5B, compare lanes 3 and 7), reflecting a more reduced state of complex I (Fig. 5B, lane 8). Nitrite-mediated improved respiration in MPP^+-treated cells is, therefore, associated with reduction of the thiol/disulfide redox equilibrium in complex I.

To clarify the mechanisms responsible for nitrite-mediated cysteine reduction in MPP^+-treated cells, we investigated activation of the major antioxidant cellular pathway Nrf2. On augmented oxidation levels—or in the presence of NO—the Nrf2 transcription factor dissociates from its cytosolic partner Keap1, translocates to the nucleus, and promotes transcription of several genes involved in the antioxidant response (1, 16, 17, 24, 72). Nitrite pretreatment in MPP^+-challenged samples—which displayed reduced cysteines in complex I (Fig. 5B)—induced S-nitrosated cysteine (SNO) modification in Keap1 (Fig. 5C, D and Supplementary Fig. S3). Nitrite administration also induced Nrf2 activation in SHSY-5Y cells overexpressing GFP-tagged Nrf2 (Fig. 6A–D). Nitrite also induced nuclear translocation of endogenous Nrf2, as evidenced by immunochemical detection in untransfected SHSY-5Y cells. Activation was also detected under physiological conditions system S-nitrosation of Keap1, as expected, and it elicited nuclear Nrf2 translocation (Fig. 6E and Supplementary Fig. S4). Collectively, these convergent data demonstrate nuclear translocation of Nrf2, which was paralleled by increased expression of known target genes (Fig. 6H, I), therefore unambiguously establishing that nitrite causes activation of the Nrf2 pathway. Activation of Nrf2 target genes was prevented, as expected, by the specific Nrf2 inhibitor trigonelline (Fig. 6G). Nrf2 nuclear translocation depended on nitrite-derived NO, as it was markedly reduced by the NO scavenger carboxy-PTIO (Fig. 6F). Nrf2 activation was not detectable in cells treated with MPP^+ alone (Fig. 6B, D, E), consistently with the unaltered levels of reduced cysteines in these samples (Fig. 5B).

Discussion

This study shows that administration of nitrite—a reservoir of bioavailable NO—is neuroprotective in several preclinical models of PD and ameliorates mitochondrial efficiency in dermal fibroblasts from PD patients. Nitrite reduces DA

neuron loss in multiple models of PD, and amelioration is not confined to prophylactic treatment. In fact, it is also observed when treatment is initiated at more advanced pathogenic stages, as evidenced in 6-OHDA rats treated 1 week after induction of the lesion. Nitrite treatment also corrects defective maximal respiratory capacity and increases proton leakage in LRRK2 mutant patients.

Our findings extend previous evidence in hypoxic settings demonstrating that nitrite is protective against ROS and complex I dysfunction (67) to normoxic conditions. Overall, the work emphasizes the role of NO signaling for proper biological function and confirms that reconstituting reserves of bioavailable NO preserves its integrity and protects against pathology (45). Importantly, reduced NO bioavailability characterizes conditions such as aging and oxidative stress, which constitute major risk factors for PD (22, 45, 69).

Our data are consistent with the notion that reactive species are essential signaling molecules—with effects that extend beyond mere toxicity and are instead essential for proper physiological function (5)—and are in agreement with evidence showing that NO exerts dichotomous effects depending on its concentration (45). Physiological NO levels ensure correct function and a moderate increase in NO may induce mild levels of stress, protecting against subsequent and more pronounced insults in a preconditioning-like manner (20). Consistently, we show that nitrite administration favors formation in complex I of S-nitrosothiols over sulfenic acid. Because the latter can be converted in higher and irreversible oxidation states (62), it is tempting to speculate that nitrite-induced S-nitrosation constitutes a molecular shield protecting cysteine residues against permanent damage *in vivo*. Further studies to test this hypothesis are warranted. Restoration of physiological NO levels can also scavenge superoxide to prevent an escalation of oxidative stress (45). Conversely, high NO levels are toxic—in fact, boosting NO production *via* iNOS is part of the innate immune response to kill invading pathogens—and are associated with neurodegeneration (52, 64). The key success factor is, therefore, restoration of NO bioavailability in a timely manner, before nitrosative/oxidative stress escalation.

Although nitrosative stress has previously been reported in PD (19), there is no evidence that exposure to NO-releasing drugs is causative or even constitutes a risk factor for this disorder. In fact, nitrosonium donors have been extensively used in clinical practice to treat cardiovascular diseases and membrane-permeable NO diffuses three dimensionally from the cell of origin, therefore conceivably reaching neurons (31, 51). Nonetheless, the use of this class of molecules is not associated with increased PD prevalence. Conversely, a recent and intriguing study highlighted an association between discontinuation of statin therapy and PD (44). Because improvement of NO bioavailability—also at the cerebral level (32)—is a well-described effect of lipophilic statins, it is tempting to speculate that decreased NO levels after therapy discontinuation might be detrimental for individuals at risk for PD.

In addition, our results demonstrating that nitrite restores mitochondrial reserve capacity and reduces proton leak in patients are consistent with similar, previous findings in healthy human subjects showing that nitrite improves mitochondrial bioenergetics (43).

Mechanistically, we demonstrate that, in normoxia, nitrite acts along two parallel and likely synergistic pathways involving complex I and Nrf2 activation. These findings are consistent with previous evidence showing that NO is an activator of the Nrf2 pathway (53) with a mechanism involving S-nitrosation of its cytosolic partner Keap1 (1, 16, 17, 24, 72). In addition, it has been recently demonstrated that, in normoxia, nitrite activates protein kinases (39), which, in turn, can activate Nrf2 (55). Overall, our findings are consistent with the notion that nitrite is a complex NO donor acting at multiple levels (33) and substantiate its therapeutic relevance given the attention that Nrf2 received as a target for neuroprotection (38). Future studies will be crucial in identifying the signaling cascades leading to nitrite-mediated Nrf2 activation and in determining whether other mitochondrial NO donors [*e.g.,* mito-SNO (20)] retain the ability to activate Nrf2.

Nitrite is a source of bioavailable NO that has been successfully used in laboratory models of cardiovascular diseases and is currently being scrutinized in clinical studies (45). In addition, currently available data support the safety of nitrite use in human therapeutics. Traditionally, nitrite has been associated with two principal health-related issues: methemoglobinemia—that is, nitrite-mediated oxidation of ferrous iron in hemoglobin to the ferric state—and an alleged carcinogenic potential. None of these issues, however, constitute a threat under the pharmacological conditions envisaged for human therapeutics. In fact, nitrite EC_{50} to induce methemoglobinemia is $\sim$1 g (54), whereas the amount used in our and other studies (46) is in the order of milligrams. Under these conditions, methemoglobinemia can be safely excluded. Conversely, there is no evidence in favor of carcinogenic activity of nitrite, as demonstrated by toxicological studies prolonging administration to 2 year periods (54) and by epidemiological investigations as well (49). In summary, nitrite pharmacokinetics, safety, and dosing features are known, and the molecule is, therefore, an excellent candidate for testing in human PD.

FIG. 6. Nitrite pretreatment promotes the activation of the antioxidant response *via* nuclear translocation of the Nrf2 transcription factor. (A) Transient GFP-Nrf2 expression in SH-SH5Y cells 24 h (*line 1*) and 48 h (*line 2*) after transfection. Empty GFP vector expression was used as control (*line 3*, 48 h after transfection). **(B, C)** Nuclear localization of GFP-Nrf2 **(B)** and GFP **(C)** after nitrite and MPP^+ treatments in SH-SY5Y transfected cells. **(D)** A representative image showing that nitrite pretreatment promotes GFP-Nfr2 translocation to the nucleus (Scale bar: 20 μm). **(E)** Nitrite-induced Nrf2 mobilization to the nucleus; translocation is exacerbated by MPP^+ treatment. **(F)** Nrf2 translocation requires bioavailability of NO because it is repressed by the NO scavenger Carboxy-PTIO. **(G)** Nuclear translocation is inhibited by treatment with the Nrf2 inhibitor trigonelline. **(H, I)** Nrf2 nuclear translocation is associated with increased expression of Nrf2 target genes. **(J)** Graphical representation modeling the temporal sequence of protein nitrosation (*green*), Nrf2 activation (*blue*), and cysteine reduction (*red*) after nitrite and/or MPP^+ administration ($*p<0.05$; $**p<0.01$; $***p<0.001$; one-way ANOVA followed by Dunnett's multiple-comparison *post doc* test). Graphs represent mean ± SEM. NO, nitric oxide.

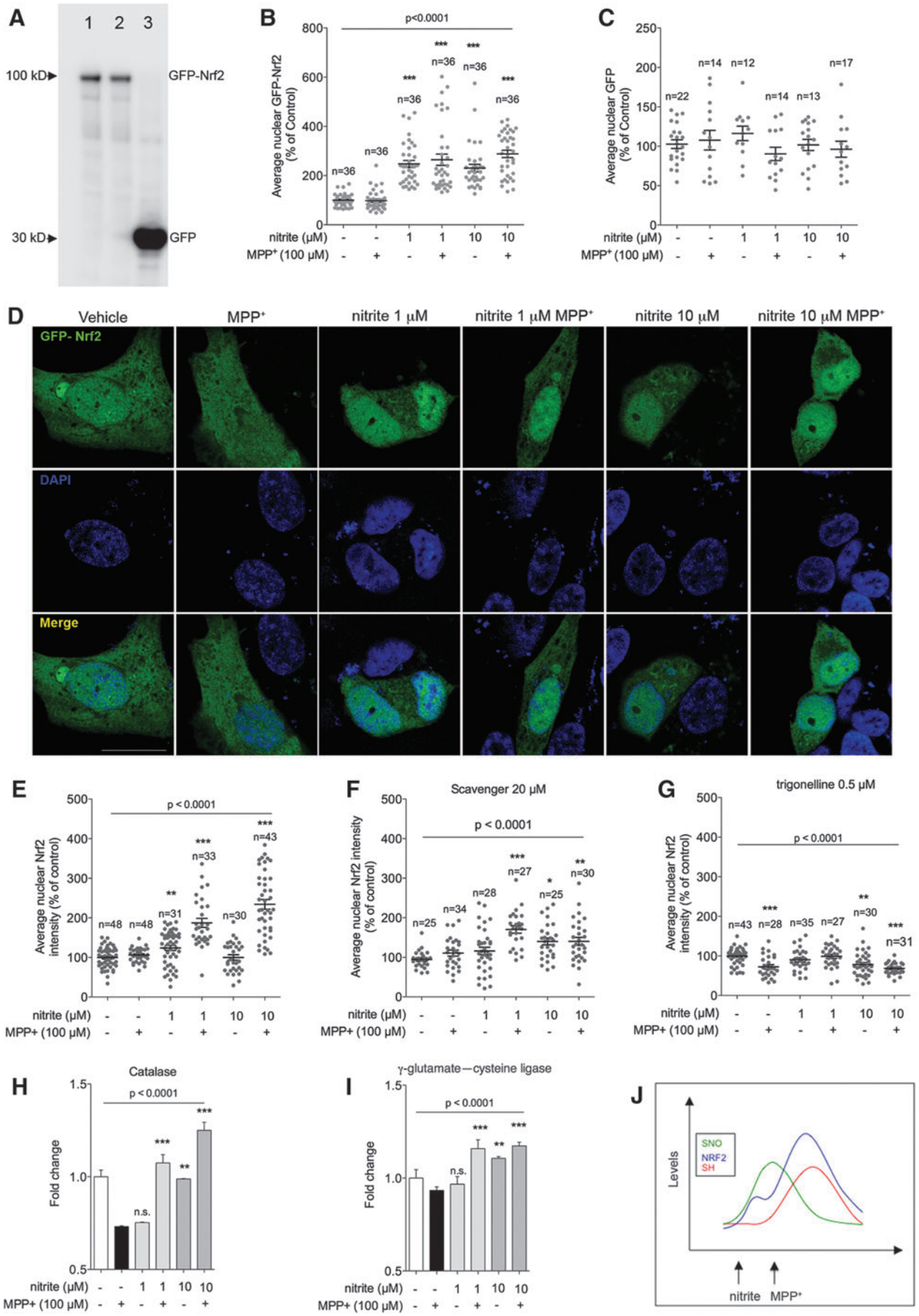

Collectively, our study demonstrates that inorganic nitrite mitigates PD pathology through a synergistic mechanism improving mitochondrial efficiency and activating the Nrf2 antioxidant pathway, and, therefore, it represents promising therapy for PD.

Materials and Methods

Chemicals

Sodium nitrite (563218), MPP^+ (D048), MPTP (M0896), Carboxy-PTIO potassium salt (NO-scavenger, C221), NOC-18 (NO-donor, A5581), 6-OHDA (H4381), oligomycin (75351), FCCP (C2920), rotenone (557368), antimycin (A8674), N-Ethylmaleimide (NEM, E3876), digitonin (D141), mannitol (M4125), glutamate (1446600), malate (4694 U), trigonelline (T5509), and 5,5-Dimethyl-1,3-cyclohexanedione (dimedone, D153303) were obtained from Sigma-Aldrich (St. Louis, MO).

Zebrafish treatment

Adult TL zebrafish were maintained at 28°C on 14/10 h light/dark cycles. Embryos were collected from natural mating and rose in E3 buffer (5 m*M* NaCl, 0.17 m*M* KCl, 0.33 m*M* $CaCl_2$, 0.33 m*M* $MgSO_4$) at 28°C.

One dpf zebrafish embryos (20 embryos/plate) were treated for 4 days with sodium nitrite (0.1–10 μM) dissolved in E3 buffer and incubated at 28°C. At day 5, fish were transferred to fresh E3 buffer and treated for two consecutive days with MPP^+ 1 m*M* as previously described (29). The solutions were daily changed. At 7dpf, zebrafish larvae were collected for behavioral testing or sacrificed to perform morphological analysis. Experiments were performed in accordance with the European Communities Council Directives (2010/63/EEC; D.L., 27.01.1992, number 116), the Dutch welfare legislation, and according to the guidelines of the Erasmus MC animal facility (EDC).

Zebrafish motor analysis

Larval motor activity was analyzed by using the *Zebralab* system (ViewPoint Life Sciences, Montreal, Quebec, Canada) as previously described (50). Viewpoint software was used in ''tracking mode'' with inactive/active and small/large thresholds, respectively, set to 0.5 and 1 mm/s. Zebrafish larvae were analyzed in a 96-well plate containing 300 μl of E3 buffer per well in a single larva/well setup. Spontaneous activity was measured at 7 dpf for hours, after 15 min of adaptation time following the transfer to the new *Zebrabox* setup.

Zebrafish whole-mount immunohistochemistry

Whole-mount immunohistochemistry was carried out as previously described (50). All incubation steps and washes were carried out on a shaker. Briefly, specimens were fixed in 4% PFA (from PFA 16%—28908; Thermo Fisher, Waltham, MA)-4% sucrose phosphate buffer saline solution (PBS—100110023; Thermo Fisher) overnight (ON) at 4°C. The next day, larvae were washed in PBS ON at 4°C. After washes, eyes and yolk sack were mechanically removed to improve antibody penetration in the brain tissue. Specimens were permeabilized with Proteinase K (PK—P2308; Sigma-Aldrich) 10 μg/ml for 15 min at room temperature (RT) and washed three times for 30 min with PBS-Triton X-100 0.2% (PBS-T). Larvae were then postfixed in 4% PFA in PBS-T for 20 min at RT and then washed three times for 10 min with PBS-T at RT. Zebrafish were then blocked with ON at 4°C in a solution containing DMSO 1% and normal goat serum 4% in PBS-T. Mouse monoclonal anti-tyrosine hydroxylase (TH, 1:500, MAB318; Millipore, Billerica, MA) incubation was performed with ON at 4°C in blocking buffer. Samples were washed five times for 30 min at RT with PBS-T and then incubated with Alexa 488 anti-mouse secondary antibody (A32723; Thermo Fisher) ON at 4°C. After five washes in PBS-T, larvae were transferred to an 80% glycerol solution and mounted for confocal analysis. Image acquisition was performed in an inverted Leica TCS SP5 confocal microscope (Leica Microsystems, Buffalo Grove, IL) in a z-stack mode, and the cell counting in the PT area was performed by analyzing all the consecutive layers of the stack using the ImageJ software.

Rotenone rat model

Male Lewis rats were treated with rotenone as previously described (18). Briefly, animals were treated up to 45 days (instead of 30). During the first 30 days, rats received an i.p. rotenone dose of 3 mg/kg/day and then, the dosage was increased to 3.5 mg/kg/day. Nitrite was administered in drinking water, 1.5 g/L, for three consecutive days before starting the rotenone treatment. Six- to 7-month-old male Lewis rats were used for all experiments (Hilltop Lab Animals, Inc., Scottdale, PA). The animals were maintained under standard conditions of temperature and humidity, in a 12 h light/dark cycle, with free access to water and food. The rats were adapted for 2 weeks before initiation of the experimental protocol. All studies were approved by the Institutional Animal Care and Use Committee at the University of Pittsburgh and were performed in accordance with published National Institutes of Health guidelines.

6-OHDA rat model

For the 6-OHDA model, male Sprague–Dawley rats (Charles River, Calco, LC, Italy) weighing 275–300 g were maintained under standard conditions of temperature and humidity with free access to food and water at the Centralized Animal Facility of the University of Pavia. Experiments were performed in accordance with the European Communities Council Directives (2010/63/EEC; D.L., 27.01.1992, number 116) and the guidelines for animal experimentation approved by the Animal Care Committees of the University of Pavia, Italy.

Animals were anesthetized by i.p. administration of 50 mg/kg of sodium-thiopental and placed in a stereotaxic frame (Stoelting, Wood Dale, IL). They received an injection of 6-OHDA (20 mg per 3 ml in saline containing 0.02% ascorbic acid) into the right striatum (1.0 mm anterior, 3.0 mm lateral, and 5.0 mm ventral with respect to bregma and dura) at 1 ml/min, using a Hamilton 10-AL syringe with a 26-gauge needle.

Twenty-week-old Sprague–Dawley rats subjected to the acute treatment were i.p. injected with 2 mg/kg of sodium nitrite in PBS 24 and 1 h before 6-OHDA injection. Animals underwent chronic treatment according to a previously reported administration paradigm (15), and received nitrite

orally, dissolved in drinking water (concentration: 50 mg/L), for 3 weeks starting 7 days after induction of the lesion.

Cell cultures

Skin dermal fibroblasts derived from PD patients bearing the G2019S (ND33879) or the N1441G (ND32975 and ND32976) LRRK2 mutations and age-matched controls were obtained from the Coriell Biorepository of the Coriell Institute for Medical Research (Camden, NJ); a detailed description is reported in Table 1. SH-SY5Y cells were obtained from Sigma-Aldrich (94030304). Cells were cultured according to standard procedures at 37°C and 5% CO_2 in DMEM medium (D6429, Sigma-Aldrich) supplemented with 10% of fetal bovine serum (F6178; Sigma-Aldrich) and 1% penicillin-streptomycin (P4333; Sigma-Aldrich). SH-SY5Y human neuroblastoma cell lines and PD-derived skin dermal fibroblast cell lines were plated and after 24 h treated for two consecutive days with sodium nitrite (1 or 10 μM) dissolved in culture medium or vehicle. For SH-SY5Y cells, on the third day, the nitrite-containing medium was removed and fresh new media containing MPP^+ 100 μM or vehicle were added to the culture for 4 h. After incubation, cells were collected for analysis.

Immunohistochemistry

Immunohistological sections were processed as previously described (37). Briefly, sections were first incubated in H_2O_2 (Sigma-Aldrich) 3% in PBS for 30 min to block internal peroxidase activity, and subsequently in PBS-T and normal horse serum (NHS) 10% for 1 h at RT. Specimens were then incubated for 24 h at 4°C with mouse monoclonal anti-TH (1:4000, MAB318; Millipore), in PBS-T and 1.5% NHS. After several washes with PBS-T, sections were incubated with biotinylated goat anti-rabbit IgG (1:500, BA 1000; Vector Laboratories, Burlingame, CA), in PBS and 1% NHS for 1 h at RT. Immuno-complexes were revealed by Vectastain Elite ABC kit (PK 4000; Vector Laboratories), using 3,3′-diamino-benzidine (DAB Substrate kit for Peroxidase, SK 4100; Vector Laboratories). Finally, sections were dehydrated and mounted with Eukitt (Kindler GmbH & Co.). Slides were observed with an Olympus BX 51(Olympus, Parkway Center Valley, PA) microscope equipped with a Leica DFC 420 camera.

Quantification of striatal TH density

Striatal lesion in DAB-stained sections was calculated as the ratio between the lesioned area, detected by the absence of TH staining, and the area of the entire TH immunopositive striatum on the injected side (6). A total of 14 sections per animals were analyzed.

Alternatively, TH density was determined by using an Odyssey infrared imaging system (LI-COR Biosciences, Lincoln, NE). Four to five serial immunofluorescence-labeled sections were scanned at 800 nm at high resolution to generate the reported average striatal DA fiber intensity as previously described (70). The dorsal region of the striatum was outlined, and the average pixel intensity for each section was obtained by using the Odyssey software (3.0).

Unbiased stereological counts

In rotenone-treated rats, an automated Nikon 90i upright fluorescence microscope equipped with five fluorescent channels and a linear encoded motorized stage was used to obtain a high-resolution montage for analysis as previously reported (71). SN images were collected at 20×(0.75 N.A.) by using a Q-imaging Retiga cooled CCD camera and the Nikon NIS-Elements software (4.2). Unbiased quantification of TH-immunoreactive cells was assessed in the SN pars compacta and reticulata from one hemisphere. All slides were scanned under the same conditions for magnification, exposure time, lamp intensity, and camera gain. After background subtraction and thresholding, quantitative analysis was determined on fluorescent images generated in three fluorescent colors (MAP2 in red; TH^+ in green, and nuclei in blue) in every sixth section throughout the entire region. An average of 11–12 sections per animal was used for quantification. Stereological counts were coded and carried out by an experimenter blinded to the treatment. The coefficient of error was calculated according to West and Gundersen as described earlier, and values were <0.10 in all cases.

In rats treated with 6-OHDA, unbiased stereological estimation of the total number of the DA cells in SNpc was made by using the optical fractionator method (75) from the STEREO INVESTIGATOR program on a Neurolucida computer-controlled microscopy system (Microbrightfield, Inc., Williston, VT). The edges of the SNc in the rostrocaudal axis were defined at all levels, with reference to a coronal atlas of the mouse brain (58). TH-positive cells in the SNc of both hemispheres were counted in every three sections, on comparable sections for all the subgroups of treatment throughout the entire nucleus. Counting frames (60×60 μm) were placed at the intersections of a grid (frame size 120×120 μm) that had been randomly placed over the section. Only counting frames for which at least a part of the frame fell within the contour of the SNpc were used for counting. Cells were marked if they were TH positive and were in focus within the counting area. Guard volumes (3 μm from the top and 3 μm from the bottom of the section) were excluded from both surfaces to avoid the problem of lost caps. The reliability of the estimate was assessed by calculation of the coefficient of error according to the formulae described in West and Gundersen (74).

Bioenergetic profiling

The Seahorse XF24 Extracellular Flux Analyzer (Agilent Technologies, Santa Clara, CA) was used to generate the bioenergetic profiles of human primary skin fibroblasts in real time and the neuroblastoma SH-SY5Y cell line as previously described (3). PD-LRRK2-derived fibroblasts and healthy controls were seeded on a Seahorse XF-24 plate at a density of 6×10^4 cells per well and grown overnight in DMEM (10% of FCS and 1% Pen-Strep) at 37°C in the presence of CO_2. The density ensures a proportional response of FCCP with cell number (3) and resulted in confluent cultures, in which cell growth was blocked by contact inhibition. After adhesion, cells were then treated for 48 h with sodium nitrite (1 or 10 μM) or vehicle (PBS) dissolved in growth medium. Media were refreshed daily. On the experimental day, cell medium was changed to unbuffered DMEM (XF Assay Medium; Agilent Technologies) supplemented with 5 mM glucose and

1 m*M* sodium pyruvate, and it was incubated for 1 h at 37°C in the absence of CO_2. Medium and reagents were adjusted to pH 7.4 on the day of the assay. After four baseline measurements for the oxygen consumption ratio, cells were sequentially challenged with injections of mitochondrial toxins: 0.5 μM oligomycin (ATP synthase inhibitor), 1 μM FCCP (mitochondrial respiration uncoupler), 0.5 μM rotenone (complex I inhibitor), and 0.5 μM antimycin (complex III inhibitor).

SH-SY5Y cells were seeded at a density of 5×10^4 cells per well and let to adhere overnight. On the next day, cells were treated for 48 h with sodium nitrite or vehicle at the same conditions as previously described for fibroblast lines. Culture medium was then removed, and cells were treated with MPP^+ 100 μM or vehicle (PBS) for 4 h at 37°C. Medium was then changed to unbuffered DMEM supplemented with 5 m*M* glucose and 1 m*M* sodium pyruvate as described and rested for 1 h at 37°C without CO2. The recovery of mitochondrial respiration was detected for 8 h (25), followed by three measurements after the injection of 1 μM FCCP, and it was used to test cell viability at the end of the assay.

Detection of protein sulfenic acid production after H_2O_2 treatment in cultured cells

Confluent SH-SY5Y cells were briefly treated (10 and 30 s) with 0.5 m*M* H_2O_2 dissolved in serum-free medium and immediately suspended in RIPA buffer containing dimedone (NaCl 150 m*M*, NP-40 1%, DOC 0.1%, sodium dodecyl sulfate [SDS] 0.1%, Tris-HCl 50 m*M*, Dimedone 1 m*M*, and protease inhibitors) (2). After 45 min of incubation in ice, protein samples were processed, separated on a NuPAGE precast sodium dodecyl sulfate polyacrylamide gel electrophoresis (SDS PAGE, NP0321; Thermo Fisher) under reducing conditions, and transferred on a PVDF membrane. The membrane was blocked for 1 h at RT in a PBS-T solution containing bovine serum albumin (BSA) 5%, and proteins were detected through the cysteine (sulfonate) polyclonal antibody (1:1000, ON at 4°C, ADI-OSA-820-F; ENZO, Farmingdale, NY) and the goat anti-rabbit HRP-conjugated secondary antibody (1:5000, P0487; DAKO-Agilent Technologies). The signal was then revealed with the ECL detection system (GE Healthcare, Barrington, IL). After detection, the membrane was washed several times with PBS-T and incubated with the anti-actin mouse primary antibody (1:4000, ON at 4°C, MAB 1501; Chemicon, Temecula, CA) and the IRDye donkey-anti-mouse secondary antibody (1:5000; Li-COR Biosciences). The signal was finally detected by using the Odyssey Imaging System (Li-COR Biosciences).

SH-SY5Y cytotoxicity assays and superoxide production

To investigate cellular toxicity in SH-SY5Y, cells were treated with nitrite dissolved in culture medium at the described concentration. After 48 h, the solution was replaced with fresh medium containing MPP^+. Cellular necrosis was evaluated after 24 h of treatment with MPP^+ with Sytox green 0.5 μM (Invitrogen, Carlsbad, CA), following the manufacturer's instructions, by using a flow cytometer (FACSaria, BD Biosciences, San Jose, CA). FlowJo Software (Tree Star, Inc., Ashland, OR) was used for data analysis. Cellular cytotoxicity was further confirmed *via* lactate dehydrogenase release (LDH colorimetric detection kit, 630117; Clonetech, Mountain View, CA). Briefly, 6×10^4 cells were seeded in a 96-well plate, treated with nitrite dissolved in DMEM (without phenol red, 21063029; Thermo Fisher) for 48 h, and finally exposed to MPP^+. After 24 h, culture medium was collected after centrifugation and then checked for lactate dehydrogenase content by following the manufacturer's guidelines.

Mitochondrial superoxide production was detected by using Mitosox Red (M36008; Invitrogen) following the manufacturer's guidelines. Briefly, after a 4 h exposure to MPP^+, 10^6 cells were harvested, quickly washed in ice-cold HBSS without Ca^{++} and Mg^{++}, and resuspendend in Hepes 0.1 *M* containing Mitosox 0.2 μM. Cells were incubated for 20 min at 37°C, protected from light, and finally analyzed with an FACSaria flow cytometer (BD Biosciences).

Detection of S-nitrosation levels in proteins

S-nitrosated proteins were detected as previously described, with minor modifications (73). Briefly, equal amounts of cells (5×10^5) were harvested *via* trypsin digestion and suspended in a lysis solution containing Tris-HCl 50 m*M*, SDS 1%, NEM 100 m*M*, and proteinase inhibitors mix (Complete mini, 11836153001; Roche, Indianapolis, IN). Lysates were incubated for 5 min at 70°C, sonicated for 15 min in a cold-water bath, and finally incubated for 30 min at RT. Protein extracts were then precipitated with a cold solution of acetone, methanol, and ethanol (50%, 25%, and 25%, respectively) suspended in the staining solution containing Tris-HCl 50 m*M*, SDS 1%, 20 μM fluorescent Alexa-NEM-800 dye (929-80020; LI-COR Biosciences) or EZ-Link PEG_2-Biotin NEM (21901BID; Thermo Fisher), ascorbate 1 m*M*, and $CuCl_2$ 1 μM and they were incubated for 1 h at RT. The staining solution was removed after acetone-methanol-ethanol precipitation and proteins were finally suspended in Tris-HCl 50 m*M*, SDS 1%, and Alexa Fluor 680 succinimidyl ester (NHS—A20008; Thermo Fisher) 20 μM. Samples were diluted in Laemni Sample buffer containing 5% B-mercaptoethanol, and proteins were separated on a NuPAGE precast SDS PAGE gel (NP0321; Invitrogen) under reducing conditions. After electrophoresis, the gel was fixed with 50% ethanol 50% and 2.5% ortophosphoric acid overnight under mild agitation. Final images and analysis were performed with the Odyssey Imaging System (Li-COR Biosciences). Immunodetection of the mitochondrial protein Ndufa9 (1:1000, ab14713; Abcam, Cambridge, MA) in the extracts processed for the S-nitrosation assay was achieved by Western blot analysis performed according to standard procedures.

Detection of SNO modification in Keap1

SNO protein modifications were detected as described in the previous paragraph by using the EZ-Link PEG_2-Biotin NEM during the staining step. Total S-nitrosylated proteins were isolated *via* the Streptavidin Mag Separose kit (28-9872-30 AA; GE Healthcare, Aurora, WI) according to the manufacturer's protocol. Briefly, equal amounts of biotin-SNO-modified proteins were incubated with 100 μl of streptavidin magnetic beads ON at 4°C under slow end-over end rotation. The biotin-streptavidin complex was then

Table 2. Primers List

Description	*Gene*	*Forward (5′-3′)*	*Reverse*
Tyrosine 3-monooxygenase/ tryptophan 5-monooxygenase activation protein, zeta polypeptide	*YWHAZ*	CCTGCATGAAGTCTGTAACTGAG	GACCTACGGGCTCCTACAACA
Ribosomal protein, large, P0	*RPLP0*	AGCCCAGAACACTGGTCTC	ACTCAGGATTTCAATGGTGCC
Catalase	*CAT*	AGATGCAGCACTGGAAGGA	CACGGGGCCCTACTGTAATA
Glutamate-cysteine ligase, catalytic subunit	*GCLC*	AGGACGTTCTCAAGTGGGG	GTCCTTTCCCCCTTCTCTTG

washed sequentially with: (1) 0.2 *M* borate pH 9, (2) 0.2 *M* sodium acetate pH 4, and (3) TBS-Urea buffer (50 m*M* Tris-HCl pH 7, 150 m*M* NaCl, and 2 *M* Urea) and biotin-SNO proteins were finally eluted in 100 μl of elution buffer (Tris-HCl 50 m*M*, 150 m*M* NaCl, SDS 2%, and 0.4% Urea) at 95°C for 10 min. Samples were then treated with 4 × Sample buffer, and 25 μl of the final solution was separated on the NuPAGE precast SDS PAGE gel and transferred on a PVDF membrane. The membrane was blocked for 1 h at RT in a PBS-T solution containing BSA 5%, and SNO-biotinylated proteins were detected for Keap1 (1:1000, ON at 4°C, 8046S; Cell Signaling, Danver, MA) and the goat anti-rabbit HRP-conjugated secondary antibody (1:5000, P0487; DAKO-Agilent Technologies). The signal was then revealed with the ECL detection system (GE Healthcare). As loading control, biotin-SNO samples were incubated with 20 μM Alexa Fluor 680 succinimidyl ester and equal amounts were separated on a NuPAGE precast SDS PAGE gel under reducing conditions. After electrophoresis, the gel was fixed with 50% ethanol and 2.5% ortophosphoric acid ON under mild agitation. Final images and analysis were performed with the Odyssey Imaging System (Li-COR Biosciences).

GFP-Nrf2 transient expression

Transient expression of the pcDNA3-EGFP-C4-Nrf2 vector (21549; Addgene, Cambridge, MA) or the vector alone was achieved in SH-SY5Y cells by using X-tremeGENE HP DNA transfection reagent (XTGHP-RO ROCHE; Sigma-Aldrich) according to the manufacturer's procedure. Twenty-four hours after transfection, cells were treated with nitrite/MPP^+ as previously described and were then collected for analysis. For IF analysis, cells were rinsed twice with PBS, then fixed 20' with PFA 4%, rinsed three times with PBS, covered with Vectashield containing DAPI (H1200; Vector Laboratories), and finally mounted on glass slides. Image acquisition was performed with a Zeiss LSM700 laser scanning confocal microscope. Alternatively, cells were lysed in Tris-HCl 50 m*M*, SDS 1%, EDTA 1 m*M*, and proteinase inhibitors (Complete Mini). Lysates were separated on a NuPAGE precast SDS PAGE gel and transferred on PVDF. The membrane was blocked for 1 h at RT in a PBS-T solution containing BSA 5%, and GFP-expressing proteins were detected with the anti-GFP antibody (1 h at RT, 1:1000, 11814460; Sigma-Aldrich) and the goat anti-mouse HRP-conjugated secondary antibody (1:5000, 715-035-150; Jackson Immuno Research, West Grove, PA). The signal was then revealed with the ECL detection system (GE Healthcare).

Complex I immunoprecipitation and detection of thiol and S-nitrosothiols

Mitochondria from SH-SY5Y neuroblastoma cells were isolated according to the ''Mitochondria Isolation Kit for Cultured Cells'' guidelines (ab110171; Abcam, Cambridge, MA), with minor modifications. Briefly, 4×10^8 confluent cells were collected by trypsin treatment and suspended in mannitol 75 m*M*, sucrose 25 m*M*, KCl 100 μM, KH_2PO_4, MgCl2 5 m*M*, Tris-HCl 20 m*M*, glutamate 5 m*M*, malate 5 m*M*, digitonin 0.01%, NEM 10 m*M*, and AlexaFluor maleimide-800 20 μM. Samples were processed three consecutive times with a homogenation step (Dounce pestle ''B,'' 30 strokes) and mitochondria collection by centrifugation at 12,000 *g*, 10 min at 4°C. Freshly isolated mitochondria were suspended in PBS, 10% maltoside, protease inhibitors, NEM 10 m*M*, and Alexa-NEM-800 dye (929-80020, LI-COR Biosciences) 20 μM at 5 mg/ml and mitochondrial complex I was immune-captured according to the ''Complex I immunocapture kit'' guidelines (ab109711; Abcam, Cambridge, MA). Isolated complex I was further processed for S-nitrosation detection assay with the addition of AlexaFluor-C2 Maleimide (NEM-680 dye, A20344; Thermo Fisher) 20 μM, ascorbate 1 m*M*, and CuCl 1 μM to the solution and incubated for 1 h at RT. Samples were finally diluted in Laemni Sample buffer containing 5% β-mercaptoethanol, and complex I proteins were separated on a NuPAGE precast SDS PAGE gel (NP0321; Invitrogen) under reducing conditions. After electrophoresis, the gel was fixed in ethanol in 50%, orto-phosphoric acid 2.5% ON under mild agitation. After image acquisition with an Odyssey Imaging System (Li-COR Biosciences), the gel was finally processed for silver staining, which was detected with a GS900 Calibrated Densitometer (Bio-Rad, Irvine, CA).

Nrf2 mobilization and evaluation of antioxidant gene transcription

Nrf2 activation was investigated in the SH-SY5Y neuroblastoma cell line. Overall, 10^5 cells were seeded on a glass coverslip, let to adhere overnight, and treated as described earlier with nitrite (48 h) and/or MPP^+ (4 h). When required, NO scavenger (Carboxy-PTIO) or the Nrf2 inhibitor trigonelline was added to culture medium at the indicated concentration. Cells were then fixed and permeabilized with PFA 4% and Triton 0.5% for 20 min at RT. Subsequently, cells were blocked with BSA 3% in PBS for 1 h at RT and incubated with the anti-Nrf2-antibody (1:100, Sc-722; Santa Cruz Biotechnology, Dallas, TX) in PBS supplemented with 1.5%

BSA ON at 4°C. After three washes with PBS, cells were incubated for 2 h at RT with a fluorescent secondary antibody (1:500, anti Rabbit Cy3 conjugated). Finally, coverslips were covered with Vectashield containing DAPI (H1200; Vector Laboratories) and mounted on glass slides. Image acquisition was performed with a Leica TCS SP5 laser scanning confocal microscope. Images were analyzed in a semi-automated fashion by using the Metamorph software (MolecularDevices, Sunnyvale, CA). The software automatically quantified the Nrf2 signal intensity-generating regions of interest around the nucleus based on the DAPI fluorescence.

Total RNA was isolated from SH-SY5Y cells treated with nitrite and MPP^+ as described earlier. Total RNA was isolated by using the RNAqueous Kit (AM1912; Ambion, Austin, TX) according to the manufacturer's directions. cDNA was synthesized with SuperScript First-Strand cDNA Synthesis Kit (11904018; Invitrogen) from 1 μg of RNA. qPCR was performed on a C1000™ Thermal Cycler, CFX96 Real-Time System (Bio-Rad) by using SYBR Green I (S7564; Invitrogen) and Platinum Taq polymerase (10966018; Invitrogen). Primer sequences were obtained from the PrimerBank PCR Primers database for Gene Expression Detection and Quantification (http://pga.mgh.harvard.edu/primerbank) and are described in Table 2. Data represent the average of values obtained from biological and experimental triplicates ± standard deviation. Expression was normalized against the average combined expression of two different housekeeping genes (Tyrosine 3-monooxygenase/tryptophan 5-monooxygenase activation protein zeta polypeptide -*YWHAZ*; and *Homo sapiens* ribosomal protein, large, *P0-RPLP0*) (14).

Statistical analysis

All values are expressed as mean ± standard error of the mean. Statistical significance was assessed by a two-sided Student's *t*-test or one-way analysis of variance followed by the Dunnett's multiple-comparison *post hoc* test. In all instances, a value of $p < 0.05$ was considered statistically different.

Acknowledgments

The authors are grateful to Dr. Peter Holland for providing constructive criticism on this article. Fundings: P.G.M. was supported by a grant from the Netherlands Genomics Initiative (NGI/NWO 05040202), a Marie Curie grant (IRG 247918), and the CEREBRAD grant under the EU-FP7 framework (project number 295552). The Extracellular Flux Analyzer by Seahorse Bioscience was purchased thanks to a generous donation from the ''Dorpmans-Wigmans Stichting'' (P.G.M.). C.M. was supported by the Ri.MED Foundation.

Dr. Gladwin receives research support from NIH grants 2R01HL098032, 1R01HL125886-01, and P01HL103455, T32 HL110849, T32 HL007563, the Institute for Transfusion Medicine and the Hemophilia Center of Western Pennsylvania.

Author Disclosure Statement

Dr. Gladwin is listed as a co-inventor on an NIH government patent for the use of nitrite salts in cardiovascular diseases, and on provisional patents for the use of recombinant neuroglobin and heme-based molecules as antidotes for CO poisoning; the former has been licensed by United Therapeutics and the latter by Globin Solutions, Inc. Dr. Gladwin is a co-investigator in a research collaboration with Bayer Pharmaceuticals to evaluate riociguate as a treatment for patients with SCD. For all other authors, no competing financial interests exist.

References

1. Abbas K, Breton J, Planson AG, Bouton C, Bignon J, Seguin C, Riquier S, Toledano MB, and Drapier JC. Nitric oxide activates an Nrf2/sulfiredoxin antioxidant pathway in macrophages. *Free Radic Biol Med* 51: 107–114, 2011.
2. Alvarez B, Carballal S, Turell L, and Radi R. Formation and reactions of sulfenic acid in human serum albumin. *Methods Enzymol* 473: 117–136, 2010.
3. Ambrosi G, Ghezzi C, Sepe S, Milanese C, Payan-Gomez C, Bombardieri CR, Armentero MT, Zangaglia R, Pacchetti C, Mastroberardino PG, and Blandini F. Bioenergetic and proteolytic defects in fibroblasts from patients with sporadic Parkinson's disease. *Biochim Biophys Acta* 1842: 1385–1394, 2014.
4. Andoh T, Chock PB, and Chiueh CC. The roles of thioredoxin in protection against oxidative stress-induced apoptosis in SH-SY5Y cells. *J Biol Chem* 277: 9655–9660, 2002.
5. Angelova PR and Abramov AY. Functional role of mitochondrial reactive oxygen species in physiology. *Free Radic Biol Med* 100: 81–85, 2016.
6. Armentero MT, Fancellu R, Nappi G, Bramanti P, and Blandini F. Prolonged blockade of NMDA or mGluR5 glutamate receptors reduces nigrostriatal degeneration while inducing selective metabolic changes in the basal ganglia circuitry in a rodent model of Parkinson's disease. *Neurobiol Dis* 22: 1–9, 2006.
7. Auburger G, Klinkenberg M, Drost J, Marcus K, Morales-Gordo B, Kunz WS, Brandt U, Broccoli V, Reichmann H, Gispert S, and Jendrach M. Primary skin fibroblasts as a model of Parkinson's disease. *Mol Neurobiol* 46: 20–27, 2012.
8. Betarbet R, Sherer TB, MacKenzie G, Garcia-Osuna M, Panov AV, and Greenamyre JT. Chronic systemic pesticide exposure reproduces features of Parkinson's disease. *Nat Neurosci* 3: 1301–1306, 2000.
9. Blandini F and Armentero MT. Animal models of Parkinson's disease. *FEBS J* 279: 1156–1166, 2012.
10. Blandini F, Levandis G, Bazzini E, Nappi G, and Armentero MT. Time-course of nigrostriatal damage, basal ganglia metabolic changes and behavioural alterations following intrastriatal injection of 6-hydroxydopamine in the rat: new clues from an old model. *Eur J Neurosci* 25: 397–405, 2007.
11. Bortolotto JW, Cognato GP, Christoff RR, Roesler LN, Leite CE, Kist LW, Bogo MR, Vianna MR, and Bonan CD. Long-term exposure to paraquat alters behavioral parameters and dopamine levels in adult zebrafish (*Danio rerio*). *Zebrafish* 11: 142–153, 2014.
12. Bretaud S, Lee S, and Guo S. Sensitivity of zebrafish to environmental toxins implicated in Parkinson's disease. *Neurotoxicol Teratol* 26: 857–864, 2004.
13. Bretaud S, MacRaild S, Ingham PW, and Bandmann O. The influence of the zebrafish genetic background on Parkinson's disease-related aspects. *Zebrafish* 8: 103–108, 2011.
14. Bruce KD, Sihota KK, Byrne CD, and Cagampang FR. The housekeeping gene YWHAZ remains stable in a model of

developmentally primed non-alcoholic fatty liver disease. *Liver Int* 32: 1315–1321, 2012.
15. Bryan NS, Calvert JW, Elrod JW, Gundewar S, Ji SY, and Lefer DJ. Dietary nitrite supplementation protects against myocardial ischemia-reperfusion injury. *Proc Natl Acad Sci U S A* 104: 19144–19149, 2007.
16. Buckley BJ, Li S, and Whorton AR. Keap1 modification and nuclear accumulation in response to S-nitrosocysteine. *Free Radic Biol Med* 44: 692–698, 2008.
17. Buckley BJ, Marshall ZM, and Whorton AR. Nitric oxide stimulates Nrf2 nuclear translocation in vascular endothelium. *Biochem Biophys Res Commun* 307: 973–979, 2003.
18. Cannon JR, Tapias V, Na HM, Honick AS, Drolet RE, and Greenamyre JT. A highly reproducible rotenone model of Parkinson's disease. *Neurobiol Dis* 34: 279–290, 2009.
19. Chinta SJ and Andersen JK. Nitrosylation and nitration of mitochondrial complex I in Parkinson's disease. *Free Radic Res* 45: 53–58, 2011.
20. Chouchani ET, Methner C, Nadtochiy SM, Logan A, Pell VR, Ding S, James AM, Cocheme HM, Reinhold J, Lilley KS, Partridge L, Fearnley IM, Robinson AJ, Hartley RC, Smith RA, Krieg T, Brookes PS, and Murphy MP. Cardioprotection by S-nitrosation of a cysteine switch on mitochondrial complex I. *Nat Med* 19: 753–759, 2013.
21. Coert BA, Anderson RE, and Meyer FB. A comparative study of the effects of two nitric oxide synthase inhibitors and two nitric oxide donors on temporary focal cerebral ischemia in the Wistar rat. *J Neurosurg* 90: 332–338, 1999.
22. Collier TJ, Kanaan NM, and Kordower JH. Ageing as a primary risk factor for Parkinson's disease: evidence from studies of non-human primates. *Nat Rev Neurosci* 12: 359–366, 2011.
23. Cooper O, Seo H, Andrabi S, Guardia-Laguarta C, Graziotto J, Sundberg M, McLean JR, Carrillo-Reid L, Xie Z, Osborn T, Hargus G, Deleidi M, Lawson T, Bogetofte H, Perez-Torres E, Clark L, Moskowitz C, Mazzulli J, Chen L, Volpicelli-Daley L, Romero N, Jiang H, Uitti RJ, Huang Z, Opala G, Scarffe LA, Dawson VL, Klein C, Feng J, Ross OA, Trojanowski JQ, Lee VM, Marder K, Surmeier DJ, Wszolek ZK, Przedborski S, Krainc D, Dawson TM, and Isacson O. Pharmacological rescue of mitochondrial deficits in iPSC-derived neural cells from patients with familial Parkinson's disease. *Sci Transl Med* 4: 141ra90, 2012.
24. Dhakshinamoorthy S and Porter AG. Nitric oxide-induced transcriptional up-regulation of protective genes by Nrf2 via the antioxidant response element counteracts apoptosis of neuroblastoma cells. *J Biol Chem* 279: 20096–20107, 2004.
25. Dranka BP, Zielonka J, Kanthasamy AG, and Kalyanaraman B. Alterations in bioenergetic function induced by Parkinson's disease mimetic compounds: lack of correlation with superoxide generation. *J Neurochem* 122: 941–951, 2012.
26. Drolet RE, Cannon JR, Montero L, and Greenamyre JT. Chronic rotenone exposure reproduces Parkinson's disease gastrointestinal neuropathology. *Neurobiol Dis* 36: 96–102, 2009.
27. Duty S and Jenner P. Animal models of Parkinson's disease: a source of novel treatments and clues to the cause of the disease. *Br J Pharmacol* 164: 1357–1391, 2011.
28. Fall CP and Bennett JP, Jr. Characterization and time course of MPP+-induced apoptosis in human SH-SY5Y neuroblastoma cells. *J Neurosci Res* 55: 620–628, 1999.
29. Farrell TC, Cario CL, Milanese C, Vogt A, Jeong JH, and Burton EA. Evaluation of spontaneous propulsive movement as a screening tool to detect rescue of Parkinsonism phenotypes in zebrafish models. *Neurobiol Dis* 44: 9–18, 2011.
30. Flinn L, Mortiboys H, Volkmann K, Koster RW, Ingham PW, and Bandmann O. Complex I deficiency and dopaminergic neuronal cell loss in parkin-deficient zebrafish (*Danio rerio*). *Brain* 132: 1613–1623, 2009.
31. Friederich JA and Butterworth JF. Sodium nitroprusside: twenty years and counting. *Anesth Analg* 81: 152–162, 1995.
32. Giannopoulos S, Katsanos AH, Tsivgoulis G, and Marshall RS. Statins and cerebral hemodynamics. *J Cereb Blood Flow Metab* 32: 1973–1976, 2012.
33. Gladwin MT, Raat NJ, Shiva S, Dezfulian C, Hogg N, Kim-Shapiro DB, and Patel RP. Nitrite as a vascular endocrine nitric oxide reservoir that contributes to hypoxic signaling, cytoprotection, and vasodilation. *Am J Physiol Heart Circ Physiol* 291: H2026–H2035, 2006.
34. Glinka Y, Tipton KF, and Youdim MB. Nature of inhibition of mitochondrial respiratory complex I by 6-Hydroxydopamine. *J Neurochem* 66: 2004–2010, 1996.
35. Glinka Y, Tipton KF, and Youdim MB. Mechanism of inhibition of mitochondrial respiratory complex I by 6-hydroxydopamine and its prevention by desferrioxamine. *Eur J Pharmacol* 351: 121–129, 1998.
36. Hill BG, Dranka BP, Zou L, Chatham JC, and Darley-Usmar VM. Importance of the bioenergetic reserve capacity in response to cardiomyocyte stress induced by 4-hydroxynonenal. *Biochem J* 424: 99–107, 2009.
37. Horowitz MP, Milanese C, Di Maio R, Hu X, Montero LM, Sanders LH, Tapias V, Sepe S, van Cappellen WA, Burton EA, Greenamyre JT, and Mastroberardino PG. Single-cell redox imaging demonstrates a distinctive response of dopaminergic neurons to oxidative insults. *Antioxid Redox Signal* 15: 855–871, 2011.
38. Jazwa A, Rojo AI, Innamorato NG, Hesse M, Fernandez-Ruiz J, and Cuadrado A. Pharmacological targeting of the transcription factor Nrf2 at the basal ganglia provides disease modifying therapy for experimental parkinsonism. *Antioxid Redox Signal* 14: 2347–2360, 2011.
39. Kamga Pride C, Mo L, Quesnelle K, Dagda RK, Murillo D, Geary L, Corey C, Portella R, Zharikov S, St Croix C, Maniar S, Chu CT, Khoo NK, and Shiva S. Nitrite activates protein kinase A in normoxia to mediate mitochondrial fusion and tolerance to ischaemia/reperfusion. *Cardiovasc Res* 101: 57–68, 2014.
40. Kaslin J and Panula P. Comparative anatomy of the histaminergic and other aminergic systems in zebrafish (*Danio rerio*). *J Comp Neurol* 440: 342–377, 2001.
41. Kordower JH, Olanow CW, Dodiya HB, Chu Y, Beach TG, Adler CH, Halliday GM, and Bartus RT. Disease duration and the integrity of the nigrostriatal system in Parkinson's disease. *Brain* 136: 2419–2431, 2013.
42. Kumari U and Tan EK. LRRK2 in Parkinson's disease: genetic and clinical studies from patients. *FEBS J* 276: 6455–6463, 2009.
43. Larsen FJ, Schiffer TA, Borniquel S, Sahlin K, Ekblom B, Lundberg JO, and Weitzberg E. Dietary inorganic nitrate improves mitochondrial efficiency in humans. *Cell Metab* 13: 149–159, 2011.
44. Lee YC, Lin CH, Wu RM, Lin MS, Lin JW, Chang CH, and Lai MS. Discontinuation of statin therapy associates

with Parkinson disease: a population-based study. *Neurology* 81: 410–416, 2013.
45. Lundberg JO, Gladwin MT, and Weitzberg E. Strategies to increase nitric oxide signalling in cardiovascular disease. *Nat Rev Drug Discov* 14: 623–641, 2015.
46. Lundberg JO, Weitzberg E, and Gladwin MT. The nitrate-nitrite-nitric oxide pathway in physiology and therapeutics. *Nat Rev Drug Discov* 7: 156–167, 2008.
47. Manzoni C, Mamais A, Dihanich S, McGoldrick P, Devine MJ, Zerle J, Kara E, Taanman JW, Healy DG, Marti-Masso JF, Schapira AH, Plun-Favreau H, Tooze S, Hardy J, Bandopadhyay R, and Lewis PA. Pathogenic Parkinson's disease mutations across the functional domains of LRRK2 alter the autophagic/lysosomal response to starvation. *Biochem Biophys Res Commun* 441: 862–866, 2013.
48. Mastroberardino PG, Orr AL, Hu X, Na HM, and Greenamyre JT. A FRET-based method to study protein thiol oxidation in histological preparations. *Free Radic Biol Med* 45: 971–981, 2008.
49. Mensinga TT, Speijers GJ, and Meulenbelt J. Health implications of exposure to environmental nitrogenous compounds. *Toxicol Rev* 22: 41–51, 2003.
50. Milanese C, Sager JJ, Bai Q, Farrell TC, Cannon JR, Greenamyre JT, and Burton EA. Hypokinesia and reduced dopamine levels in zebrafish lacking beta- and gamma1-synucleins. *J Biol Chem* 287: 2971–2983, 2012.
51. Miller MR and Megson IL. Recent developments in nitric oxide donor drugs. *Br J Pharmacol* 151: 305–321, 2007.
52. Moncada S and Bolanos JP. Nitric oxide, cell bioenergetics and neurodegeneration. *J Neurochem* 97: 1676–1689, 2006.
53. Motohashi H and Yamamoto M. Nrf2-Keap1 defines a physiologically important stress response mechanism. *Trends Mol Med* 10: 549–557, 2004.
54. National Toxicology Program. Toxicology and carcinogenesis studies of sodium nitrite (CAS NO. 7632-00-0) in F344/N rats and B6C3F1 mice (drinking water studies). *Natl Toxicol Program Tech Rep Ser* 495: 7–273, 2001.
55. Niture SK, Khatri R, and Jaiswal AK. Regulation of Nrf2-an update. *Free Radic Biol Med* 66: 36–44, 2014.
56. Panov A, Dikalov S, Shalbuyeva N, Taylor G, Sherer T, and Greenamyre JT. Rotenone model of Parkinson disease: multiple brain mitochondria dysfunctions after short term systemic rotenone intoxication. *J Biol Chem* 280: 42026–42035, 2005.
57. Panula P, Sallinen V, Sundvik M, Kolehmainen J, Torkko V, Tiittula A, Moshnyakov M, and Podlasz P. Modulatory neurotransmitter systems and behavior: towards zebrafish models of neurodegenerative diseases. *Zebrafish* 3: 235–247, 2006.
58. Paxinos G and Franklin KBJ. *The Mouse Brain in Stereotaxic Coordinates*. Amsterdam, The Netherlands: Elsevier Academic Press, 2004.
59. Przedborski S and Vila M. The 1-methyl-4-phenyl-1,2,3,6-tetrahydropyridine mouse model: a tool to explore the pathogenesis of Parkinson's disease. *Ann N Y Acad Sci* 991: 189–198, 2003.
60. Raat NJ, Shiva S, and Gladwin MT. Effects of nitrite on modulating ROS generation following ischemia and reperfusion. *Adv Drug Deliv Rev* 61: 339–350, 2009.
61. Ramsay RR, Salach JI, and Singer TP. Uptake of the neurotoxin 1-methyl-4-phenylpyridine (MPP+) by mitochondria and its relation to the inhibition of the mitochondrial oxidation of NAD+-linked substrates by MPP+. *Biochem Biophys Res Commun* 134: 743–748, 1986.
62. Reddie KG and Carroll KS. Expanding the functional diversity of proteins through cysteine oxidation. *Curr Opin Chem Biol* 12: 746–754, 2008.
63. Rink E and Wullimann MF. The teleostean (zebrafish) dopaminergic system ascending to the subpallium (striatum) is located in the basal diencephalon (posterior tuberculum). *Brain Res* 889: 316–330, 2001.
64. Ryan SD, Dolatabadi N, Chan SF, Zhang X, Akhtar MW, Parker J, Soldner F, Sunico CR, Nagar S, Talantova M, Lee B, Lopez K, Nutter A, Shan B, Molokanova E, Zhang Y, Han X, Nakamura T, Masliah E, Yates JR, 3rd, Nakanishi N, Andreyev AY, Okamoto S, Jaenisch R, Ambasudhan R, and Lipton SA. Isogenic human iPSC Parkinson's model shows nitrosative stress-induced dysfunction in MEF2-PGC1alpha transcription. *Cell* 155: 1351–1364, 2013.
65. Sallinen V, Torkko V, Sundvik M, Reenila I, Khrustalyov D, Kaslin J, and Panula P. MPTP and MPP+ target specific aminergic cell populations in larval zebrafish. *J Neurochem* 108: 719–731, 2009.
66. Sherer TB, Betarbet R, Stout AK, Lund S, Baptista M, Panov AV, Cookson MR, and Greenamyre JT. An in vitro model of Parkinson's disease: linking mitochondrial impairment to altered alpha-synuclein metabolism and oxidative damage. *J Neurosci* 22: 7006–7015, 2002.
67. Shiva S, Sack MN, Greer JJ, Duranski M, Ringwood LA, Burwell L, Wang X, MacArthur PH, Shoja A, Raghavachari N, Calvert JW, Brookes PS, Lefer DJ, and Gladwin MT. Nitrite augments tolerance to ischemia/reperfusion injury via the modulation of mitochondrial electron transfer. *J Exp Med* 204: 2089–2102, 2007.
68. Tanner CM, Kamel F, Ross GW, Hoppin JA, Goldman SM, Korell M, Marras C, Bhudhikanok GS, Kasten M, Chade AR, Comyns K, Richards MB, Meng C, Priestley B, Fernandez HH, Cambi F, Umbach DM, Blair A, Sandler DP, and Langston JW. Rotenone, paraquat, and Parkinson's disease. *Environ Health Perspect* 119: 866–872, 2011.
69. Tanner CM, Ross GW, Jewell SA, Hauser RA, Jankovic J, Factor SA, Bressman S, Deligtisch A, Marras C, Lyons KE, Bhudhikanok GS, Roucoux DF, Meng C, Abbott RD, and Langston JW. Occupation and risk of parkinsonism: a multicenter case-control study. *Arch Neurol* 66: 1106–1113, 2009.
70. Tapias V, Cannon JR, and Greenamyre JT. Pomegranate juice exacerbates oxidative stress and nigrostriatal degeneration in Parkinson's disease. *Neurobiol Aging* 35: 1162–1176, 2014.
71. Tapias V, Greenamyre JT, and Watkins SC. Automated imaging system for fast quantitation of neurons, cell morphology and neurite morphometry in vivo and in vitro. *Neurobiol Dis* 54: 158–168, 2013.
72. Um HC, Jang JH, Kim DH, Lee C, and Surh YJ. Nitric oxide activates Nrf2 through S-nitrosylation of Keap1 in PC12 cells. *Nitric Oxide* 25: 161–168, 2011.
73. Wang X, Kettenhofen NJ, Shiva S, Hogg N, and Gladwin MT. Copper dependence of the biotin switch assay: modified assay for measuring cellular and blood nitrosated proteins. *Free Radic Biol Med* 44: 1362–1372, 2008.
74. West MJ and Gundersen HJ. Unbiased stereological estimation of the number of neurons in the human hippocampus. *J Comp Neurol* 296: 1–22, 1990.

75. West MJ, Slomianka L, and Gundersen HJ. Unbiased stereological estimation of the total number of neurons in the subdivisions of the rat hippocampus using the optical fractionator. *Anat Rec* 231: 482–497, 1991.

Address correspondence to:
Dr. Pier G. Mastroberardino
Department of Molecular Genetics
Erasmus MC
Wytemaweg 80
Rotterdam 3015 CN
The Netherlands

E-mail: p.g.mastroberardino@erasmusmc.nl

Dr. Chiara Milanese
Department of Molecular Genetics
Erasmus MC
Wytemaweg 80
Rotterdam 3015 CN
The Netherlands

E-mail: c.milanese@erasmusmc.nl

Date of first submission to ARS Central, January 11, 2017; date of final revised submission, August 10, 2017; date of acceptance, August 13, 2017.

Abbreviations Used

6-OHDA = 6-hydroxydopamine
DA = dopaminergic
dpf = days postfertilization
EDC = Erasmus MC animal facility
H_2O_2 = hydrogen peroxide
NEM = N-Ethylmaleimide
NHS = normal horse serum
NO = nitric oxide
NOC-18 = 3,3-Bis(aminoethyl)-1-hydroxy-2-oxo-1-triazene
OCR = oxygen consumption rate
ON = over night
PBS = phosphate buffer saline
PD = Parkinson's disease
PK = Proteinase K
PT = posterior tuberculum
ROS = reactive oxygen species
RT = room temperature
SDS = sodium dodecyl sulfate
SDS PAGE = sodium dodecyl sulfate polyacrylamide gel electrophoresis
SH = reduced cysteines
SNO = S-nitrosated cysteines
SNpc = *substantia nigra* pars compacta
TH = tyrosine hydroxylase
TL = Tupfel long fin